DETECTION OF MINOR APPLE DAMAGE BASED ON HYPERSPECTRAL IMAGING
/
基于高光谱图像的苹果轻微损伤检测方法

Yu Shi, Lei Yan, Jiaxin Liu, Lei Pang, Jiang Xiao* [1]
Beijing Forestry University, Beijing, 100083/China;
Tel: 18201112198; E-mail: xiaojiang56@126.com
DOI: https://doi.org/10.35633/inmateh-58-22

Keywords: *minor apple damage, hyperspectral image, PCA, ROC, SVM*

ABSTRACT

In order to detect apples with minor damages quickly and efficiently, which is essential for grading of apples and improving fruit quality, a method based on hyperspectral imaging and a SVM (support vector machine) model was proposed. First, to actualize this model, black-and-white correction and brightness correction based on the near-sphere geometry were applied to the apple hyperspectral image, which reduced the noise interference in the spectral image and corrected the uneven brightness distribution so that the damaged parts of the apple were easy to detect. Second, four effective wavelengths from the full-spectrum spectral data were selected via PCA (principal component analysis) and ROC (receiver operating characteristic) curve analysis. Third, the SVM model was trained using a total of 800 sets of data, which referenced the mean brightness values of intact and damaged areas in the spectral images utilizing the effective wavelengths. Additionally, 160 sets of data were employed to test the accuracy of the damage identification model. Finally, the SVM model was trained using all the samples to identify damage in 360 sets of apple images using the effective wavelengths, and the damaged areas were marked onto the apple's visible-light image. The detection accuracy for the premium, first-class and second-class apples was 90.8%, 88.3% and 87.5%, respectively, with an average detection accuracy of 88.9%. These experimental results indicated that the developed procedures were conducive to more accurate and effective detection of minor apple damage.

摘要

苹果轻微损伤检测对于苹果分级和提升果品整体质量至关重要，为了快速高效地检测出苹果轻微损伤，提出了一种基于高光谱图像和支持向量机的苹果轻微损伤检测方法。首先，对采集到的苹果高光谱图像使用黑白校正、基于近球体的亮度校正，减弱光谱图像中的噪声干扰、校正苹果图像亮度分布的不均匀，使苹果的损伤区域易于检测；其次，对苹果全谱段光谱数据利用主成分分析和受试者工作特征曲线分析法选择 4 个有效波长（488nm、529nm、632.8nm 和 970nm）；再次，利用有效波长下苹果光谱图像中完好和损伤区域的平均亮度值共 800 组数据训练支持向量机模型，并使用 160 组数据对模型进行损伤判定准确率检验；最后，使用全部样本训练支持向量机模型并对 360 组有效波长下苹果图像进行识别，将判断为损伤的区域标记到苹果的可见光图像中。特级苹果的检测准确率为 90.8%、一级苹果的检测准确率为 88.3%、二级苹果的检测准确率为 87.5%，平均检测准确率为 88.9%。实验结果表明，利用黑白校正和基于近球体的亮度校正后处理后的苹果高光谱图像，并针对由主成分分析和受试者工作特征曲线分析法选择出的 4 个有效波长，通过支持向量机模型进行分类，能够准确、有效的检测出苹果的轻微损伤。

INTRODUCTION

Apples are often slightly damaged during the picking and selling process *(Juan X., et al., 2005)*, which can cause the whole fruit to rot and result in serious loss during storage and transportation, especially during the later storage period *(Mehl P. M., et al., 2002)*. At present, there is still a large gap between China and developed countries with respect to the post-harvest detection of fruit, as in most areas of China the fruits are only manually classified in accordance with such measures as size and weight *(Su D.L. et al., 2012)*. Such methods of manual grading present low work efficiency and low precision and can easily result in cross-infection *(Li J.B., 2015)*. In the early 1970s, machine imaging technology was introduced and applied in the field of quality inspection for agricultural products *(Liu H.L., 2015)*. This technology features high accuracy, stability, and efficiency and can be applied to conduct a quality inspection of the fruit's surface, greatly reducing labour costs and error rates, and a number of studies have been performed in an effort to advance this technology

[1] *Yu Shi, As. Master Stud; Lei Yan, Associate Prof. Ph.D.; Jiaxin Liu, Master Stud; Lei Pang, Master Stud; Jiang Xiao, Prof. Ph.D.*

further. In 2005, *Juan X. et al., (2005)* used a hyperspectral imaging system of the wavelength range of 400–1000 nm for detecting bruises on 'Jonagold' apples. *ElMasry G. et al., (2008)* used a hyperspectral technique in the near-infrared region to detect early mechanical damage on the surface of apples of different colours. In 2011, by combining hyperspectral technology with infrared thermal imaging, *Piotr B. et al., (2011)* detected early damage to apples and demonstrated that the spectral images in a broad spectral range (400 - 5000 nm) can detect the location and depth of the damage. In 2012, *Yasasvy N. et al.* (2012) calculated the ratio of the damaged area relative to the intact area of strawberries and evaluated the edible part of the strawberry using a multi-band fusion strategy. In China, *Zhao J.W. et al., (2009)* demonstrated that hyperspectral imaging technology can detect quality of apples and *Shan J.J. et al. (2011)* detected damage to the apple's surface and calculated the damaged area by means of hyperspectral imaging techniques. *Huang W.Q., et al. (2013)* selected two effective wavelengths (i.e., 820 nm and 970 nm) for detecting slightly damaged apples and developed a multi-spectral algorithm for identifying such damage. *Jiang J.B. et al., (2016)* used the hyperspectral EESA non-destructive testing model to detect and identify the minor mechanical damage to "Yellow Banana" and "Yantai Fuji" apples and *Liu J.J. et al. (2016)* used a second-order Butterworth high-pass filter to filter hyperspectral images at the wave band of 640 nm to detect the external damage of apples. In this paper, based on hyperspectral image technology, the detection of minor damage to apples was conducted using black-and-white correction and brightness correction based on the near-sphere geometry, analysis and selection of the effective wavelengths by PCA and ROC curves, and establishing a corresponding SVM model in order to realize the rapid and effective detection of slightly damaged apples and to mark the damaged areas.

MATERIALS AND METHODS

● Sample preparation

In this study, Fuji apples from Shandong Province were used as the research objects. These apples had red and yellow surfaces whose slightly damaged areas were difficult to detect by simple visual inspection. There were a total of 45 apple samples, all of which were premium apples with no obvious defects on their surfaces. The damaged areas were made using a ball with a mass of 99.62 g. The ball was dropped about 35 cm away from the surface of the apple using a falling ball impact test machine, thus hitting the surface of the apple to generate a damaged area that was difficult to observe via the naked eye. As shown in Fig. 1, the damage preparation meets the requirements of the Apple Grade Specification (NY/T1793-2008) promulgated by the Ministry of Agriculture of the People's Republic of China in 2009. For grading of the apples, an intact apple was considered premium, an apple with one damaged area was first-class, and an apple with two damaged areas was categorized as second-class.

a) Premium apple *b) First-class apple* *c) Second-class apple*

Fig. 1 - Apple sample

● Hyperspectral image acquisition

The hyperspectral image acquisition system used in this study is shown in Figure 2. The system consisted of a hyperspectral imager (SOC710VP), a lens (Schneider XENOPLAN 17mm/5.6), a light source (CL150 halogen lamps), a stage and a computer (ThinkCenter, Intel (R) Core(TM) i5-3470 CPU @ 3.20GHz, RAM4.0GB). A set of 150W halogen lamps fixed to both sides of the camera was used as a light source to emit a stable, continuous band of parallel light to the surface of apple placed on the stage. The CCD camera built into the hyperspectral imager was used to scan the apple images within the wave band of 400-1000nm. The apple images had a spectral resolution of 4.68nm and a total of 128 bands.

All of the apple samples used in this study were placed on the stage against the lens, keeping the apple still during the imaging process. Every apple was photographed three times before being damaged, rotating the apple 120° for each shot to ensure that the entire apple image was acquired. Subsequently, the apple was hit once using the falling ball impact test machine to form a damaged area and the hyperspectral image was acquired again. Finally, another hyperspectral image was acquired after the apple had acquired a second damaged area.

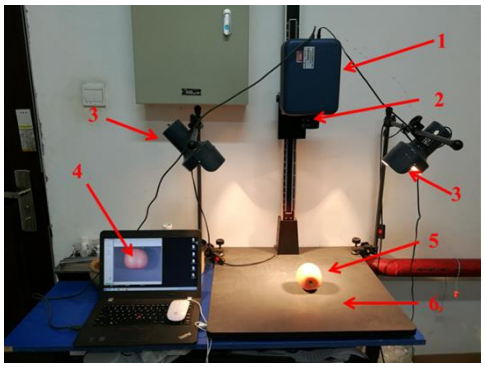

Fig. 2 - The acquisition system for hyperspectral imaging

1 - Hyperspectral imager; 2 - Lens; 3 - A set of parallel light sources; 4 - Computer; 5 - Experimental sample; 6 – Stage

- **Image correction**

After the process of image acquisition, the acquired hyperspectral images needed to undergo black-and-white correction due to the uneven distribution of light intensity in each wave band, which was caused by the different responses of the photosensitive cells in the push-scan type near-infrared hyperspectral imager *(Zhang B.H., et al., 2015)*. The formula used for black-and-white correction was as follows:

$$I_R = \frac{I_{R0} - I_{RD}}{I_{RW} - I_{RD}} \times DN \tag{1}$$

Where *IR* is the hyperspectral reflectance image calibrated by black-and-white correction, *IR0* is the original hyperspectral image, *IRW* is the all-white reference image, *IRD* is the all-black reference image, and *DN* is the maximum brightness value of the image of 4096. The all-white reference image was obtained from a standard Teflon whiteboard with a reflectance of 99%, and the all-black reference image was taken with the lens covered. In this study, calibration was performed using a standard gray board of the Munsell colour N5 (model: 710-2079). A visible light image before and after being corrected is shown in Figure 3.

a) Before being corrected *b) After being corrected*

Fig. 3 - Visible light image before and after black and white correction

Because of the uneven brightness distribution of the apple due to its spherical shape, the brightness in the centre of the apple was high and the brightness of the edge area was low. Therefore, a brightness correction method for a near-sphere model was used to eliminate the uneven brightness distribution of the apple surface. The correction formula was as follows:

$$IMG_{Ratio} = \frac{IMG}{IMG_{Idea1}} \times 255 \tag{2}$$

Where the IMG_{Ratio} is the ratio image between a single wavelength image and the ideal brightness model, *IMG* is the near-infrared image at this wavelength, and IMG_{Ideal} is the ideal brightness model. In order to adapt the ideal brightness model to the size and boundary shape of the apple being inspected, the brightness model also underwent a masking process. The result of the brightness correction method is shown in Fig. 4.

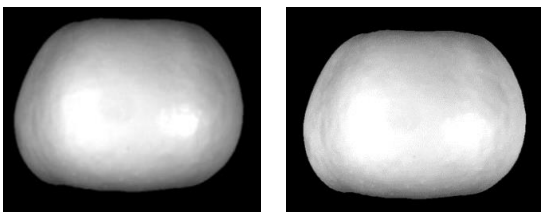

a) Before brightness correction *b) After brightness correction*

Fig. 4 - Brightness correction based on a nearly spherical shape

As it can be seen in Figure 4, the brightness distribution in the apple area is more even after undergoing brightness correction. This is especially true for the pixels in the edge region, as the defects in the edge and the central region remain relatively low after correction, which makes the defects less likely to be confused with the edge regions. This process helps facilitate the detection of defects, particularly defective regions at the edges of the image.

RESULTS

- **Region of interest**

In order to obtain the reflection spectrum of the intact and damaged area of the apple, as shown in Fig. 5, the damaged *ROIs* (Region of interest) were selected from damaged areas of the first-class and second-class apples. Additionally, intact *ROIs* were selected from intact areas of the premium, first-class and second-class apples.

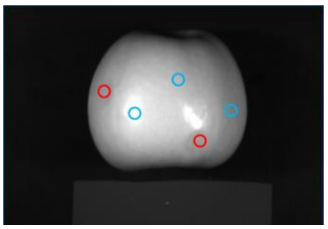

Fig. 5 - The position selection of an apple's ROI

The average spectral values of the damaged and intact areas were calculated using the reflection spectrum information of all the pixels in the *ROI* and representative results were shown in Fig. 6.

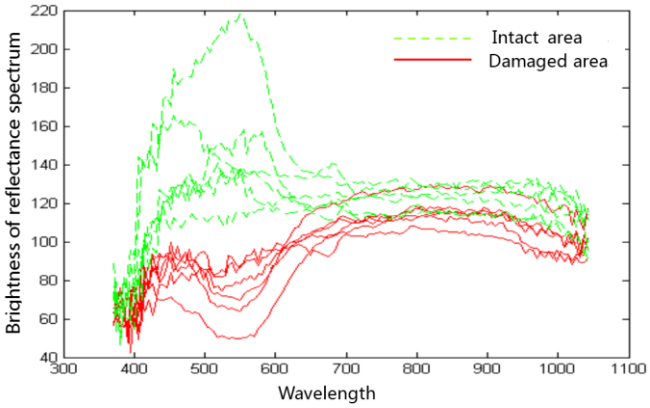

Fig. 6 - Average spectral value of the apple's ROI

It can be seen from the average spectral curves of the damaged and the non-damaged areas in Fig. 6 that they were significantly different in the spectral range of 400-700 nm. Therefore, this result demonstrated that it was feasible to identify the damaged area of an apple using spectral information.

- **PCA of the full-band spectrum**

In this study, PCA was used to analyse the average spectral values of the intact *ROI* and damage *ROI* of apples in the spectral range of 400-1000 nm at various wavelengths. The first seven principal components were obtained according to their contribution rate, as shown in Fig. 7.

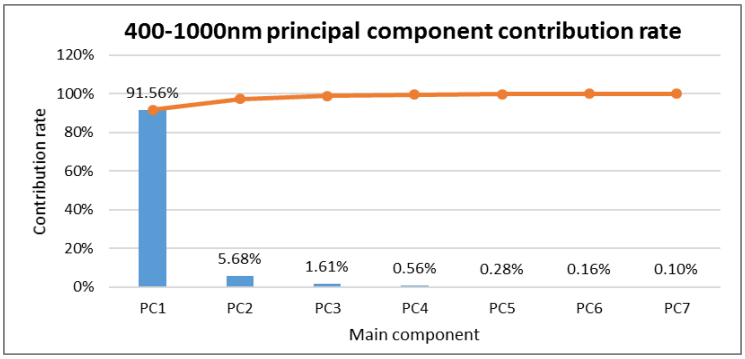

Fig. 7 - Contribution rate coefficient related to the PCA of the full-spectrum

It can be seen from Figure 7 that the cumulative contribution rate of the first two principal components reached more than 95%, including most of the information in the hyperspectral image. The hyperspectral image was reconstructed using the first four principal components and this reconstructed image was shown in Fig. 8. It can be seen from the figure that the *PC1* image retained most of the information of the 128 original band images and it was easier to distinguish the intact and damaged areas of the apple in this image. In *PC2*, it can be seen that the contour area of the apple was higher than the overall brightness, and this unevenness reflected the edge information of the apple, but this had no obvious relationship regarding the judgment of apple damage. It can be clearly seen in the *PC3* image that there were reflective area and light colour area which was inconsistent with the colour of apple's surface, reflecting the colour information of apple's surface, and this could be applied to judge the reflective area of the apple. In PC4, the texture information, including spots on the surface of the apple, was predominantly retained.

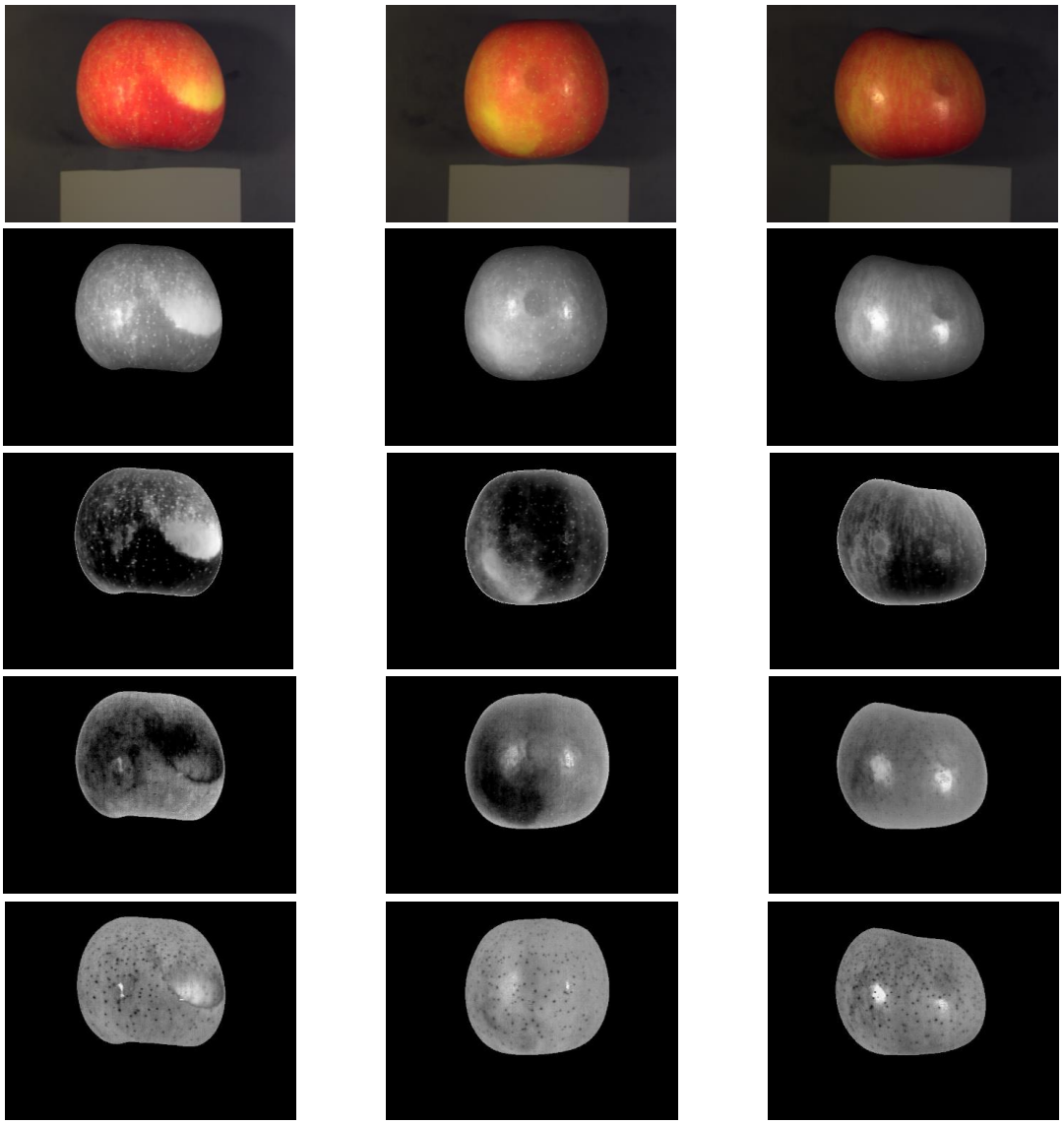

a) Premium apple *b) First-class apple* *c) Second-class apple*

Fig. 8 - Visible images of the PC1-PC4 reconstructions

Subsequently, we used the apple image of the first principal component as the basis for damage determination and compared the weight coefficients of the respective wavelengths to obtain their distributions in the first principal component, as shown in Fig. 9.

The weight coefficients of each wavelength band in *PC1* were all positive; therefore, the two wavelengths of 529 nm and 970 nm whose weight coefficients were the local maximums were selected as the most effective wavelengths.

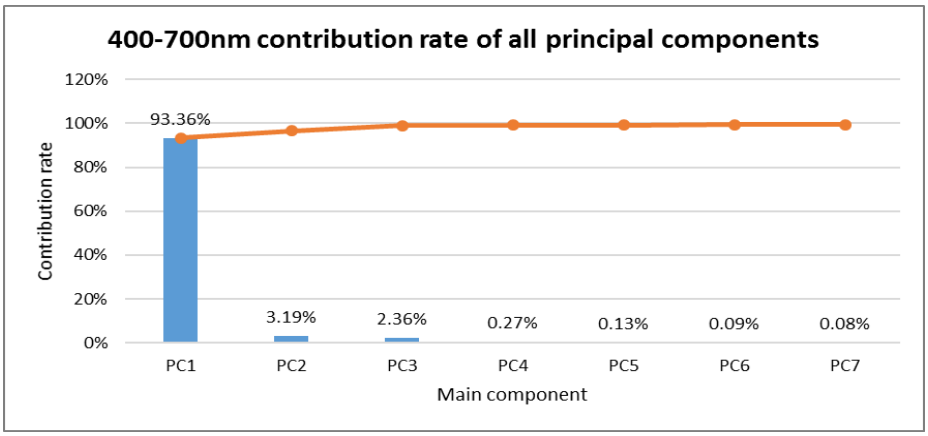

Fig. 9 - PC1 distribution of the weight coefficient

- **PCA of the 400-700 nm spectral segment**

It can be seen from the average spectral value of the apple's *ROI* in Fig. 6 that the average spectral values of the damaged and non-damaged areas of the apple varied greatly from 400 nm to 700 nm. Therefore, in this study, the data for this spectral region was also analyzed by PCA alone and the contribution rate of the first seven principal components was shown in Fig. 10. The cumulative contribution rate of the first two principal components was over 95%, which included most of the information in the hyperspectral image.

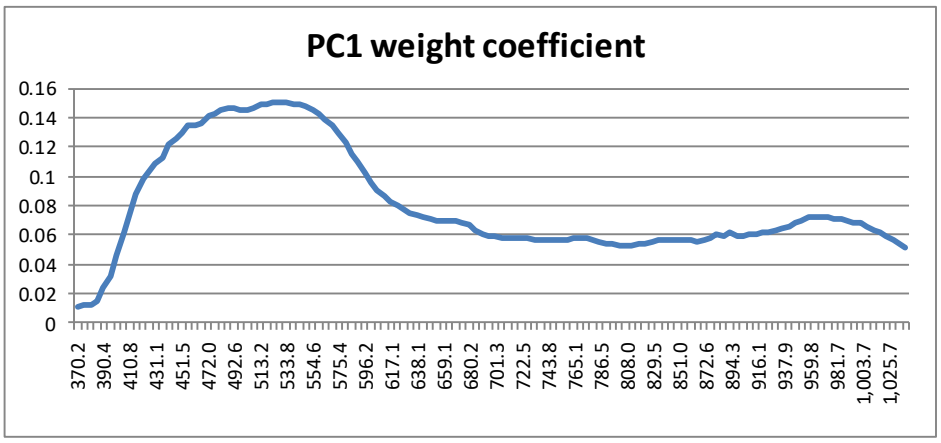

Fig. 10 - Contribution rate of PCA analysis in the 400-700 nm wave band

PC1 was also selected as the basis for apple damage determination in the spectral range of 400-700nm. *PC1* was calculated by linear superposition of the spectral images of 58 bands and the *PC1* weight distribution coefficient in the 400-700nm spectral interval was shown in Fig. 11. In the wavelength range of 400-700 nm, the weight coefficients of each band in *PC1* were positive, and there was only one obvious peak on the weight coefficient distribution curve. Therefore, the wavelength of 488 nm, where the weight coefficient was the local maximum, was selected as the effective wavelength.

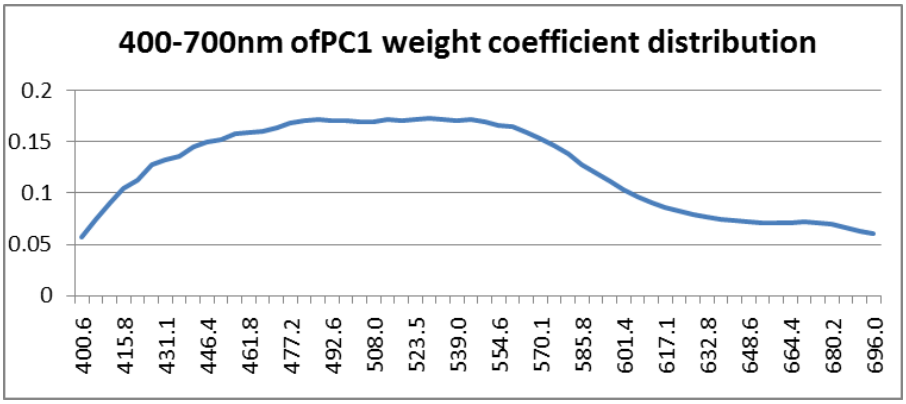

Fig. 11 - Distribution of PC1 weight coefficients at 400-700 nm

- **Effective wavelength selection based on the ROC curve**

In order to judge the correlation between the spectral reflectance image and the damage information for the apples at each wave band, the *ROC* curve was employed to analyse the spectral values of the *ROI* for all the spectral segments and the results are shown in Fig. 12.

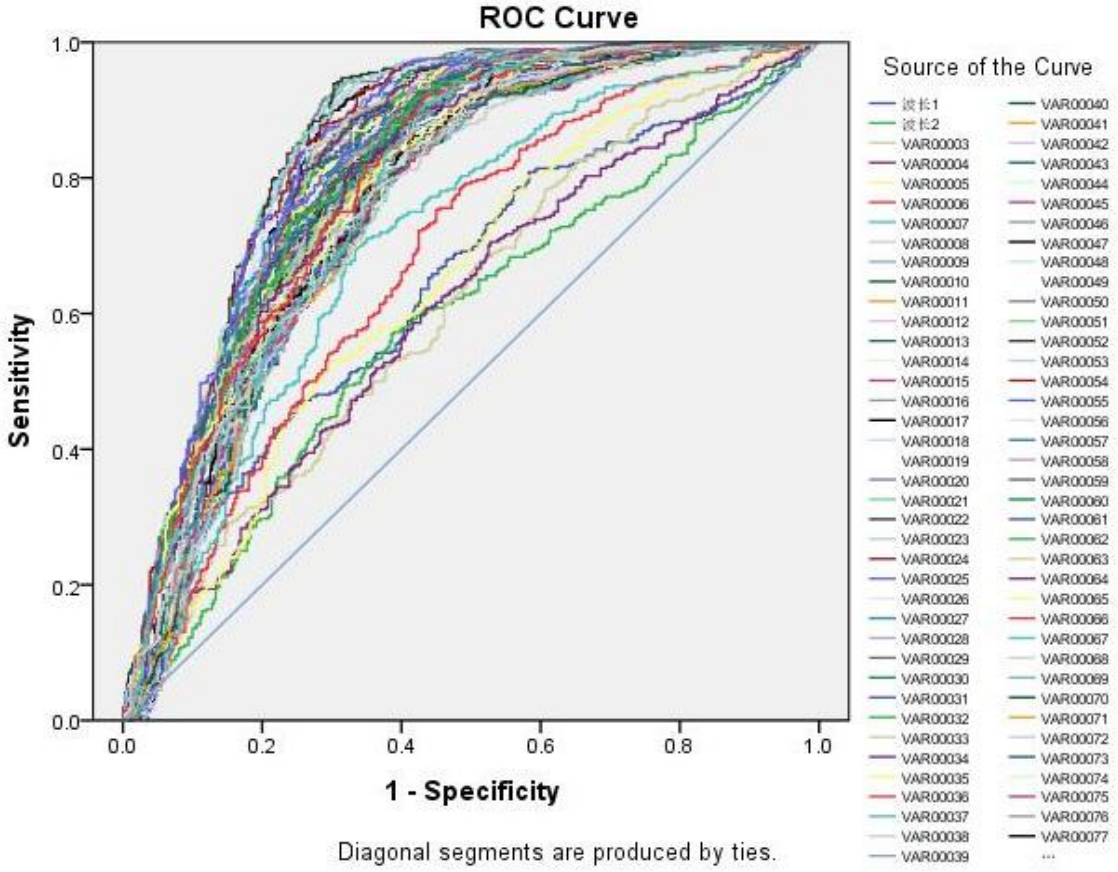

Fig. 12 - Comparison of the classification effects for the full-band spectral segment of the ROC

The area under the *ROC* curve for each principal component was calculated and the classification accuracy of the full-band spectral segment at the optimal threshold was obtained. The optimal classification accuracy of the different bands was plotted as a curve, as shown in Fig. 13.

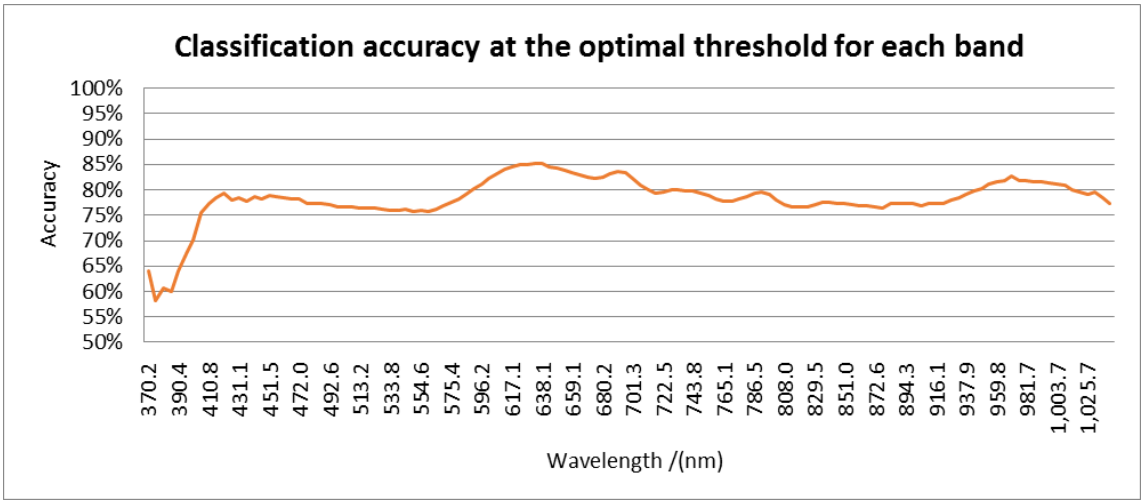

Fig. 13 - Classification accuracy at the optimal threshold for each band

The classification accuracy of each band was spread between 55% and 90%, and there were a total of 38 wavelength spectrums the classification accuracy of which was over 80%, respectively, each locating in the wavelength range of 590-712 nm or 948-1092 nm.

Among these, the wavelength at the curve peak was the same wavelength determined by the *ROC* curve to accurately determine the damage areas of the apple in the spectrum image. The highest accuracy for identifying apple damage relative to the spectral reflectance image was obtained at the wavelength of 632.8 nm, which demonstrated an accuracy of 85.2%.

In the process of determining the optimal wavelength for detection of apple damage and in order to find the optimal wavelength combination, both the accuracy of the detection and the distance between the various bands should be taken into account. After comprehensively assessing the above two factors, the wavelengths of 632.8nm and 970nm were selected as the most effective wavelengths, which, together, demonstrated a classification accuracy of more than 80%.

- **The SVM model for the detection of minor apple damage**

After selecting the effective wavelength, the amount of data required for apple damage detection was only 1/32 of the original hyperspectral data volume, indicating that the amount of data required was greatly reduced. This study chose *SVM* as the classification model for specific wavelength information. In order to verify the accuracy of the damage determination using the *SVM* model, the intact and damaged area images were selected for testing. The intact *ROI* was randomly selected from the surface of the premium fruit, and the damage *ROI* was selected from the damaged areas distributed on the first-class and second-class apples. Among these, 500 intact *ROI*s and 300 damaged *ROI*s (total of 800 sets of data) randomly selected were used as the training group samples. Additionally, 100 intact *ROI*s and 60 damaged *ROI*s (a total of 160 sets of data) were used as test group samples. The model training and testing processes were repeated three times, the accuracy for damage determination was counted and the average value was calculated as the accuracy for determination of minor apple damage for the *SVM* model, as shown in Table 1.

Table 1

The determination accuracy for minor apple damage using the SVM model

Group	1	2	3	average value
Training group	800	800	800	800
Test group	160	160	160	160
Misjudgement of intact	7	12	5	8
Misjudgement of damage	6	8	4	6
Intact accuracy /%	93%	88%	95%	92%
Damage accuracy /%	90%	86.7%	93%	90%
Total misjudgement	13	20	9	14
Accuracy/%	91.875%	87.5%	94.875%	91.25%

According to the three results, that easily meets the requirements for detection of minor apple damage.

The process of detecting and marking the damaged area of the apple was as follows:

(1) The average brightness value of all the apple *ROI*s was used as a training sample to train the *SVM* classification model.

(2) To read the mask image corresponding to the apple sample, a 10*10 sliding window was constructed to traverse the entire image (step size = 5), and the sliding window coordinates located in the apple area were recorded, as shown in Fig. 14.

Fig. 14 - 10*10 sliding window area

(3) The average brightness value of reflectance spectrum image of each apple sample at the effective wavelength in each sliding window area was then calculated.

(4) All the data of the obtained single apple sample was inputted into the trained *SVM* classifier and each sliding window area was classified as intact or not, with the sliding window coordinate range marked as damaged being recorded.

(5) The position marked as the damaged area in the visible light image of the sample was then circled.

(6) The apple images were classified according to the number of damaged areas.

Representative results of the damaged area detection for the apples are shown in Fig. 15.

Fig. 15 - Results of the damaged area detection for the apples

The images of 120 sets of intact apples, 120 sets of apples with one damaged area and 120 sets of apples with two damaged areas, with a total of 360 sets, were assessed using this damage detection method. The detection accuracy for premium, first-class, and second-class apples was 90.8%, 88.3%, and 87.5%, respectively, resulting in an average detection accuracy of 88.9%.

CONCLUSIONS

By using black-and-white correction and brightness correction based on near-sphere geometry, the noise interference in the apple hyperspectral images was reduced and the unevenness of the image brightness distribution was corrected, so that the damaged area of the apple was easier to detect.

The full-spectral analysis and spectral analysis of the 400-700nm range were performed on the hyperspectral images via *PCA* and two wavelengths were selected that demonstrated large contribution rates in *PC1*. Moreover, the two wavelengths with the highest accuracy for damage determination were selected via ROC curve analysis from the full-band spectrum. The effective wavelengths for detecting minor apple damage were thus determined to be 488 nm, 529 nm, 632.8 nm and 970 nm, and this information was successfully selected to reduce the amount of redundant information and improve the detection efficiency of the process.

The classification accuracy of the spectral data under the effective wavelengths was tested via the *SVM* model. A total of 160 samples were randomly selected and the average accuracy of the three tests was 91.25%, which supports the feasibility of this method. The average spectral values in 360 sets of apple images at effective wavelengths were selected to train the *SVM* classification model and the detection of minor apple damage based on the *SVM* classification model was performed. The damaged area was then marked onto the apple's visible light image. The overall average detection accuracy for the three types of apple images was 88.9% and the experimental results showed that this detection method based on hyperspectral image and *SVM* model could accurately and effectively detect the presence of minor damage towards apples.

ACKNOWLEDGEMENT

This study was supported by the National Natural Science Foundation of China (No.31770769).

REFERENCES

[1] ElMasry G. et al., (2008), Early detection of apple bruises on different background colours using hyperspectral imaging, *LWT-Food Science and Technology*, Vol. 41, Issue 2, pp.337-345, Elsevier Science, Amsterdam / Netherlands;

[2] Huang W.Q., Chen L.P., Li J.B. et al., (2013), Effective wavelengths determination for detection of slight bruises on apples based on hyperspectral imaging, *Transactions of the Chinese Society of Agricultural Engineering*, Vol. 29, Issue 01, pp.272-277, Chinese Society of Agricultural Engineering, Beijing / China;
[3] Jiang J.B., You D., Wang G.P. et al., (2016), Study on the Detection of Slight Mechanical Injuries on Apples with Hyperspectral Imaging, *Spectroscopy and Spectral Analysis*, Vol. 36, Issue 07, pp.2224-2228, Chinese Optical Society, Beijing / China;
[4] Juan X., Cédric B., Pál T., et al., (2005), Detecting Bruises on 'Golden Delicious' Apples using Hyperspectral Imaging with Multiple Wavebands, *Biosystems Engineering*, Vol. 90, Issue 1, pp.27-36, Elsevier Science, San Diego / USA;
[5] Juan X., JosseDe B., et al., (2005), Bruise detection on 'Jonagold' apples using hyperspectral imaging, *Postharvest Biology and Technology*, Vol. 37, Issue 2, pp. 152-162, Elsevier Science, Amsterdam / Netherlands;
[6] Li J.B., Huang W.Q., Zhao C.J., (2015), Machine vision technology for detecting the external defects of fruits — a review, *The Imaging Science Journal*, Vol. 63, Issue 5, pp.241-251, Taylor & Francis Online, London / England;
[7] Liu H.L., (2015), *Study of Pear Surface Defects Detection Based on Laser Speckle Image*, Zhejiang University, Zhejiang / China;
[8] Liu J.J, Liu F.L., Shi T., et al., (2016), Detection of External Damage of Apple by Hyperspectral Image Technique, *Journal of Chinese Institute of Food Science and Technology*, Vol. 18, Issue 01, pp.278-284, Chinese Institute of Food Science and Technology, Beijing / China;
[9] Mehl P. M., Chao K., Kim M., et al., (2002), Detection of Defects on Selected Apple Cultivars Using Hyperspectral and Multispectral Image Analysis, *Applied Engineering in Agriculture*, Vol. 18, Issue 2, pp.219-226, American Society of Agricultural Engineers, St Joseph / USA;
[10] Piotr B., Wojciech M., Jpanna W. et al., (2011), Detection of early bruises in apples using hyperspectral data and thermal imaging, *Journal of Food Engineering*, Vol. 110, pp.345-355, Elsevier SCI, Oxford / England;
[11] Su D.L., Li G.Y., He J.X. et al., (2012), Progress in application of near infrared spectroscopy to non-destructive detection of big yield fruits' quality in China, *Science and Technology of Food Industry*, Vol. 33, Issue 06, pp.460-464, Beijing Industrial Technology Research Institute, Beijing / China;
[12] Shan J.J., Peng Y.K., Wang W., et al., (2011), Simultaneous Detection of External and Internal Quality Parameters of Apples Using Hyperspectral Technology, *Transactions of the Chinese Society of Agricultural Machinery*, Vol. 42, Issue 03, pp.140-144, Chinese Society for Agricultural Machinery and Chinese Academy of Agricultural Machinery Sciences, Beijing / China;
[13] Yasasvy N., Ruplal C., Lalit G. et al. (2012), A decision-fusion strategy for fruit quality inspection using hyperspectral imaging, *Biosystems Engineering*, Vol. 111, Issue 1, pp.118-125, Springer, New York / USA;
[14] Zhang B.H., Li J.B., Zheng L.,(2015), Development of a Hyperspectral Imaging System for the Early Detection of Apple Rottenness Caused by Penicillium, Journal of Food Process Engineering, Vol. 38, Issue 5, pp.499-509, Wiley-Blackwell Publishing, Malden/ USA;
[15] Zhao J.W., Saritporn V., ., Chen S.Q., et al., (2009), Nondestructive measurement of sugar content of apple using hyperspectral imaging technique, Maejo International Journal of Science and Technology, Vol. 3, Issue 01, pp.130-142, Maejo University, Chiang Mai / Thailand.